Kinetics and Spectroscopic Evidence That the Cu(I)−Semiquinone Intermediate Reduces Molecular Oxygen in the Oxidative Half-Reaction of *Arthrobacter globiformis* Amine Oxidase[†]

Eric M. Shepard, Kristina M. Okonski, and David M. Dooley*

Department of Chemistry and Biochemistry, Montana State University, Bozeman, Montana 59717

Received June 19, 2008; Revised Manuscript Received October 9, 2008

ABSTRACT: The role of copper during the reoxidation of substrate-reduced amine oxidases by O_2 has not yet been definitively established. Both outer-sphere and inner-sphere pathways for the reduction of O_2 to H_2O_2 have been proposed. A key step in the inner-sphere mechanism is the reaction of O_2 directly with the Cu(I) center of a Cu(I)−semiquinone intermediate. To thoroughly examine this possibility, we have measured the spectral changes associated with single-turnover reoxidation by O_2 of substrate-reduced *Arthrobacter globiformis* amine oxidase (AGAO) under a wide range of conditions. We have previously demonstrated that the internal electron-transfer reaction [Cu(II)−TPQ_{AMQ} → Cu(I)−TPQ_{SQ}] (where TPQ_{AMQ} is the aminoquinol form of reduced TPQ and TPQ_{SQ} is the semiquinone form) occurs at a rate that could permit the reaction of O_2 with both species to be observed on the stopped-flow time scale [Shepard, E. M., and Dooley, D. M. (2006) *J. Biol. Inorg. Chem. 11*, 1039−1048]. The transient absorption spectra observed for the reaction of O_2 with substrate-reduced AGAO provide compelling support for the reaction of the Cu(I)−TPQ_{SQ} form. Further, global analysis of the kinetics and the transient absorption spectra are fully consistent with an inner-sphere reaction of the Cu(I)−semiquinone intermediate with O_2 and are inconsistent with an outer-sphere mechanism for the reaction of the reduced enzyme with O_2.

Amine oxidases catalyze the oxidative deamination of primary amines to aldehydes, with the concomitant reduction of O_2 to H_2O_2. Copper-containing amine oxidases can be divided into two subclasses depending on the modified tyrosine residue present in the active site: 2,4,5-trihydroxyphenylalanine quinone (TPQ,[1] EC 1.4.3.6) or lysine tyrosylquinone (LTQ, EC 1.4.3.13). The TPQ cofactor is formed by the post-translational six-electron oxidation of a conserved tyrosine residue, while LTQ is formed by means of the oxidation and cross-linking of a tyrosine and a lysine residue. Formation of both cofactors is a self-processing event requiring only copper and molecular oxygen (*1*−*4*).

The TPQ-containing amine oxidases (CuAOs) are widely distributed in nature, having a multitude of physiological roles, including, but not limited to, hormone biosynthesis, detoxification, cell growth, signaling, histamine metabolism, lymphocyte adhesion, and adipocyte maturation (*5*−*12*). Over the past decade, the determination of multiple CuAO crystal structures has provided insight into the nature of substrate and substrate analogue specificity, the biogenesis of the TPQ cofactor, and the enzyme mechanism (*13*−*20*). All the structurally characterized CuAOs are homodimers with molecular masses ranging from 140 to 240 kDa and contain a single active site per monomer composed of a mononuclear type II copper ion and the TPQ cofactor (*21*−*23*).

Amine oxidases utilize a ping-pong bi bi mechanism divided into two half-reactions:

$$E_{ox} + RCH_2NH_2 \rightleftarrows E{-}RCH_2NH_2 \rightarrow E_{red} + RCHO \quad (1)$$

$$E_{red} + O_2 + H_2O \rightarrow E_{ox} + H_2O_2 + NH_3 \quad (2)$$

The oxidation of primary amines to aldehydes is conventionally termed the reductive half-reaction (eq 1; Scheme 1, **A** → **B**). The critical step in this half-reaction is abstraction of a proton from the α-carbon of the amine substrate carried out by an absolutely conserved aspartate acting as a general base. Reoxidation of the organic cofactor is known as the oxidative half-reaction (eq 2) and is diagrammed in Scheme 1 (**B** → **E**). With the release of aldehyde, the reduced enzyme exists as an equilibrium between the two-electron-reduced aminoquinol state [Cu(II)−TPQ_{AMQ}] (**B**) and the one-electron-reduced semiquinone state [Cu(I)−TPQ_{SQ}] (**C**), with the magnitude of K_{eq} being highly dependent upon the temperature and enzyme source (*24*). The two-electron oxidation of the reduced enzyme by O_2 (producing H_2O_2) yields the iminoquinone form of TPQ (**E**, TPQ_{IMQ}), which may undergo hydrolysis liberating NH_3 and the resting cofactor (**A**, TPQ_{OX}) (*15*).

[†] This research was supported by Grant GM 27659 (D.M.D.) from the National Institutes of Health.

* To whom correspondence should be addressed. E-mail: dmdooley@montana.edu. Telephone: (406) 994-4371. Fax: (406) 994-7989.

[1] Abbreviations: AGAO, *Arthrobacter globiformis* amine oxidase; BPAO, bovine plasma amine oxidase; CuAO, copper- and TPQ-containing amine oxidase; ECAO, *Escherichia coli* amine oxidase; EPR, electron paramagnetic resonance; HPAO, *Hansenula polymorpha* amine oxidase; k_{ET}, electron-transfer rate; LTQ, lysine tyrosylquinone; β-PEA, β-phenylethylamine; PSAO, pea seedling amine oxidase; TPQ, 2,4,5-trihydroxyphenylalanine quinone; TPQ_{AMQ}, aminoquinol form of TPQ; TPQ_{IMQ}, iminoquinone form of TPQ; TPQ_{IMQ340}, intramolecular hydrogen-bonded iminoquinone form of TPQ; TPQ_{IMQ450}, iminoquinone form of TPQ lacking the intramolecular H-bond; TPQ_{OX}, oxidized form of TPQ; TPQ_{RED}, reduced form of TPQ existing in equilibrium between TPQ_{AMQ} and TPQ_{SQ}; TPQ_{SQ}, semiquinone form of TPQ.

10.1021/bi8011516 CCC: $40.75
Published on Web 12/03/2008

Scheme 1: Proposed CuAO Catalytic Mechanism Illustrating the Two Proposed Pathways for Cofactor Reoxidation

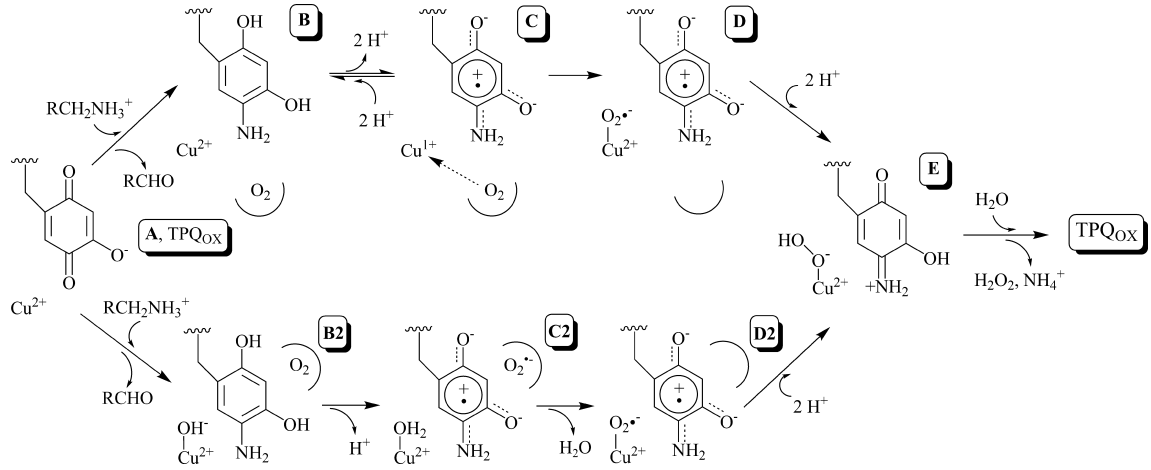

Significant questions remain with regard to which species initially reduces O_2 and whether the reoxidation mechanism differs for CuAOs purified from various sources. The two most plausible reoxidation mechanisms are detailed in Scheme 1. In one proposal, the initial reduction of O_2 occurs by an inner-sphere reaction with Cu(I) (Scheme 1, **C**), resulting in a Cu(II)-bound superoxide species (**B** → **D**) (*24*−*26*). This proposal circumvents the spin conversion problem associated with two-electron reduction reactions of oxygen (*27*) and is substantiated by the ample precedence for the reactivity of three-coordinate Cu(I) sites with O_2 in copper-containing metalloproteins (*28*−*30*). Furthermore, detailed kinetics studies of the CuAO from lentil seedlings strongly supported the participation of the Cu(I)−TPQ_{SQ} intermediate in the reduction of O_2 (*31, 32*).

Additional support for an inner-sphere mechanism for reoxidation comes from metal substitution experiments in *Arthrobacter globiformis* amine oxidase (AGAO) (*33*). Co(II)- and Ni(II)-substituted AGAO displayed $k_{cat}(O_2)$ values that were ∼1% of that of the wild-type, Cu(II)-containing enzyme. Kishishita et al. (*33*) suggested that their data may be consistent with either an outer-sphere mechanism, (where TPQ_{AMQ} directly reduces O_2) or an inner-sphere mechanism. Given the significant rate advantage of the native, copper-containing enzyme compared to the metal-substituted forms, based on facile copper redox chemistry certainly appears plausible (*33*). The kinetic advantage of the copper-containing enzyme is consistent with the [Cu(I)−TPQ_{SQ}] species as a viable intermediate.

In contrast, results obtained using the amine oxidases from *Hansenula polymorpha* (HPAO) and bovine plasma (BPAO) were consistent with an outer-sphere mechanism, thereby leading to the second proposal detailed in Scheme 1 (**B2** → **D2**) (*34*−*37*). These studies suggest that O_2 binds in a hydrophobic pocket near the quinone cofactor and the first electron-transfer reaction occurs via a classical outer-sphere step between TPQ_{AMQ} and O_2 [**B2** → **C2** (rate-limiting step)], with the [Cu(I)−TPQ_{SQ}] intermediate existing off-pathway, in equilibrium with species **B2** (the Cu(I)-semiquinone is not depicted in the **B2** → **D2** pathway for the sake of clarity). The superoxide anion that is generated in the hydrophobic pocket then migrates to the Cu(II) center (**C2** → **D2**) (*38*).

Notably, the flash-frozen structure of catalytically competent *Escherichia coli* amine oxidase (ECAO) crystals following aerobic exposure to excess β-PEA reveals a dioxygen species bound to copper in a side-on fashion (*39*). The Cu−O−O bond angle of 88° is suggestive of a peroxide product, indicating that the cofactor is in the iminoquinone state. The observed peroxide species bridges the copper and TPQ cofactor, which could be consistent with electron transfer occurring from either TPQ_{AMQ} or Cu(I) (*39, 40*).

It is clear that additional kinetics and spectroscopic experiments on structurally characterized CuAOs are necessary to define the reoxidation mechanism(s) and to probe the possibility that CuAOs from different sources are mechanistically distinct. Tanizawa and co-workers had previously demonstrated that AGAO is an excellent subject for investigating the oxidative half-reaction under single-turnover conditions (*41*). We carried out stopped-flow experiments as a function of pH, temperature, and O_2 concentration using a photodiode array detector to collect spectra as a function of time. In contrast to the previously published results (*41*), global data analysis of our data demonstrates that an inner-sphere mechanism is operative in which the Cu(I)−TPQ_{SQ} intermediate in AGAO reacts with O_2 but is inconsistent with the direct reaction of TPQ_{AMQ} with O_2 in an outer-sphere process.

MATERIALS AND METHODS

Enzyme Purification. Our published procedure for overexpression of recombinant Strep-tagged AGAO in *E. coli* cells (*42*) was modified to eliminate catalase, thus simplifying the purification of AGAO. *E. coli* catalase-depleted cells (BL21 DE3 CD03) were kindly provided by K. Tanizawa (*33*). The AGAO-Strep vector (pAGAOst) was then transformed into BL21 CD03 cells. The CD03 cells produced AGAO as effectively as the BL21 cells with production of only trace levels of catalase. Enzyme purification followed our published procedure (*42*) except that the final ultragel column was eliminated because this column was previously employed to separate catalase from AGAO. Generally, ∼80−90 mg of purified AGAO was obtained from 4 L of cell culture. The purified protein is highly homologous and displays kinetics and spectroscopic properties identical to those of Strep-tagged AGAO (*42*) (E. M. Shepard, K. M. Hilmer, and D. M. Dooley, unpublished results). Moreover, quantification of TPQ content accomplished via titration with

phenylhydrazine (*43*) reveals preparations to consistently titrate 1.44 ± 0.02 TPQs per dimer.

Sample Preparation. All measurements were taken in 100 mM potassium phosphate buffer (pH 7.2 or 8.2). For the experiments in D_2O buffer, tribasic potassium phosphate was dissolved in D_2O (99.9 atom % for deuterium, Aldrich). The pD of the solution was then decreased by addition of DCl (35 wt % solution in D_2O, 99 atom % for deuterium, Aldrich) to a final pD of 8.25. All enzyme, substrate, and buffer solutions were transferred to sealed glass vials and thoroughly purged with Ar gas passed through a vanadium bubbler, HCO_3, H_2O setup (*44*) for 3 h. Solutions in D_2O were purged with only Ar gas to prevent any deuterium isotope exchange with the H_2O present in the vanadium bubbler setup. When anaerobic, all solutions were transferred to a Coy anaerobic chamber (Coy Laboratories, Grass Lake, MI).

Separate 10 mL buffer solutions in glass vials were equilibrated with O_2 to monitor reoxidation rates at distinct O_2 concentrations. The first solution was bubbled with O_2 gas for 30 min at 5 °C, yielding a final O_2 concentration of ∼1.40 mM, while the second solution was allowed to equilibrate with atmospheric O_2 at 5 °C, producing a final O_2 concentration of ∼300 μM, as calculated on the basis of published oxygen solubility tables (*45*). Each vial was subsequently sealed and transferred to the Coy anaerobic chamber. After buffers had been mixed in a 1:1 ratio with enzyme solutions in the stopped-flow instrument, as described below, these buffers yield solutions with final O_2 concentrations of 700 and 150 μM, respectively.

Substrate-reduced enzyme was prepared by addition of a 5-fold excess of β-phenylethylamine (β-PEA) (over active site concentration) and allowed to incubate for 20 min. An excess of β-PEA was utilized to ensure full reduction of the TPQ cofactor, in contrast to previous stopped-flow studies with AGAO (*41*). To ensure that single-turnover conditions were achieved for stopped-flow studies, excess β-PEA was removed by running the anaerobic, substrate-reduced enzyme sample (following the incubation period) over a 5 mL PD-10 column (Pharmacia) that was equilibrated with 12 column volumes of anaerobic buffer (performed in the anaerobic chamber). Elution was accomplished by addition of anaerobic buffer. Fractions were collected by visual inspection, as the reduced enzyme is intensely yellow in color. The main protein fraction (∼1 mL) was collected and subsequently utilized for stopped-flow experiments. UV−vis spectral analysis of all fractions conclusively demonstrated the separation of excess β-PEA from enzyme.

Stopped-Flow Measurements. Stopped-flow measurements were performed at 5, 10, and 20 °C with an Applied Photophysics SX.18MV photodiode-array stopped-flow spectrophotometer. To maximize the signal-to-noise ratio, the light guide was directly coupled to the lamp housing using a coupling device (Applied Photophysics). This effectively doubled the intensity of the lamp signal reaching the photodiode array in the 300−330 nm region.

To ensure anaerobic conditions were maintained during experimentation, the sample handling unit of the stopped-flow setup was housed inside the Coy anaerobic chamber, which was thoroughly purged of O_2 (as monitored with an O_2 sensor) via the use of N_2/H_2 gas mix in the presence of a Coy catalyst box. The thermostatted water bath utilized to control the temperature of the sample handling unit was thoroughly purged with N_2 gas. Immediately prior to experimentation, the drive syringes on the sample handling unit were flushed with ∼40 mL of anaerobic buffer. Equal volumes of the enzyme and buffer solutions were mixed, and spectra were recorded at every 1.28 ms in a wavelength region of 300−700 nm.

To confirm that full TPQ reduction was achieved and to obtain a control spectrum (see below), the enzyme sample from the PD-10 column elution was loaded into the sample handling unit of the stopped-flow system using a Hamilton gastight syringe. Another gastight syringe containing anaerobic buffer was loaded. Spectral analysis of the reduced enzyme/anaerobic buffer mixture was then conducted for 500 ms. The anaerobic buffer was then immediately flushed out of the drive syringe on the sample handling unit and replaced with buffer containing ∼1.4 mM O_2. Spectral changes accompanying the oxidative half-reaction were then recorded. Upon acquisition of data, the 1.4 mM O_2 buffer was then immediately flushed out of the drive syringe on the sample handling unit and replaced with the 300 μM O_2 buffer, at which time it was thoroughly flushed through the observation cell and data were again acquired. To ensure experimental reproducibility, three to four data sets at each oxygen concentration were obtained. In all cases, the results were highly reproducible.

Following the acquisition of data, files were exported in ASCII format. Spectra in the absence of O_2 displayed the absorbance features characteristic of the TPQ_{SQ} moiety for the time course of the control experiment (500 ms). An individual spectrum from this data file was then inserted into the 700 and 150 μM O_2 data files as the initial $t = 0$ ms spectrum. The purpose of this was to establish a true starting point for the spectral changes associated with cofactor reoxidation. These measures were required because upon exposure of the reduced enzyme to O_2, significant spectral changes occur during the dead time (1.1 ms) of the stopped-flow instrument.

Data Analysis. Potential reaction models for the oxidative half-reaction were examined using a global analysis software package (Pro-Kineticist II, Applied Photophysics). To minimize variables during the global analysis process, known spectra were entered into the Pro-Kineticist program for certain intermediate quinone and copper species along the reaction path. To summarize, anaerobically reduced CuAOs exist in an equilibrium between Cu(II)−TPQ_{AMQ} (Scheme 1, **B**) and Cu(I)−TPQ_{SQ} species (Scheme 1, **C**) (*24*). The TPQ_{SQ} moiety displays a unique absorption spectrum with λ_{max} values at ∼360, 440, and 470 nm (*24*−*26, 33, 46*), while the neutral TPQ_{AMQ} (Scheme 1, **B**) has a λ_{max} at ∼315 nm, with a featureless absorption spectrum in the visible region (*47*).

K_{eq} values for the Cu(II)−TPQ_{AMQ} ⇆ Cu(I)−TPQ_{SQ} equilibrium in AGAO have been experimentally determined at room temperature for pH 7.2 and 8.2 (*48*). The K_{eq} values presented in Table 1 represent an average of the values obtained via extrapolation from a van't Hoff plot constructed from our previous measurements (*48*) and direct estimation of K_{eq} from experimental absorbance values using a ε_{480} of 1700 M^{-1} cm^{-1} for TPQ_{OX} (*38*) and a ε_{468} of 4500 M^{-1} cm^{-1} for TPQ_{SQ} (*48*). The ε_{468} for TPQ_{SQ} in AGAO was independently determined by titration of substrate-reduced enzyme with cyanide (20-fold excess over copper). CN^- binds Cu(I),

Table 1: Kinetic Parameters for the Internal Redox Equilibrium [Cu(II)−TPQ_{AMQ} ⇆ Cu(I)−TPQ_{SQ}] in AGAO

pH	temp (°C)	K_{eq}	k_{ET} (s^{-1})[a]	k_{-1} (s^{-1})[a]
7.2	5	0.29	73 ± 6	252 ± 20
7.2	10	0.33	82 ± 7	243 ± 20
7.2	20	0.48	106 ± 10	219 ± 19
8.2	10	0.35	35 ± 2	101 ± 5

[a] The reported error values in k_{ET} and k_{-1} assume that the error in k_{obs} from temperature jump relaxation measurements is equally shared (*48*).

thereby shifting the Cu(II)−TPQ_{AMQ} ⇆ Cu(I)−TPQ_{SQ} equilibrium toward the latter species (*49*). Utilizing a factor of 1.4 reactive quinone species per dimer, on the basis of titration of the oxidized enzyme with phenylhydrazine, a ε_{468} value of 4400 M^{-1} cm^{-1} was obtained for TPQ_{SQ}. The calculation of k_{ET} and k_{-1} from respective K_{eq} values assumes that the experimentally determined k_{obs} ($k_{ET} + k_{-1}$) for relaxation of reduced AGAO following a temperature jump is approximately independent of temperature. The availability of K_{eq} for the intramolecular equilibrium, ε_{310} for a TPQ_{AMQ} model compound (*33*), and ε_{468} for TPQ_{SQ} enabled deconvolution of the fully reduced enzyme (TPQ_{RED}) spectrum (see above) into the component TPQ_{AMQ} and TPQ_{SQ} moieties under the majority of experimental conditions tested. Experiments conducted in D_2O are the exception as the effects of deuterium on the parameters listed in Table 1 are unknown. The deconvoluted TPQ_{AMQ} and TPQ_{SQ} files were appended with species concentration values and loaded into the Pro-K software program as separate fixed files, representing the contributions from each species to the $t = 0$ ms spectrum (TPQ_{RED}). Additionally, rate constants k_{ET} and k_{-1} (Table 1) were fixed during the model minimization process. A similar approach has recently been utilized in the global analysis of spectral changes accompanying the reductive half-reaction in AGAO (*50*).

Rate constants were obtained by fitting single-wavelength difference absorbance changes to a first-order rate equation using Origin 7.0 (Microcal). Absorbance increases at 488 nm (pH 8.2 and pD 8.25 data) and 499 nm (pH 7.2 data) were not cleanly fit with a single-exponential equation from 0 to ~20 ms. The appearance of an isosbestic point after the initial phase (see Results) supported the use of a double-exponential fit for the full time series. Accordingly, absorbance changes at these wavelengths were fit with a biphasic exponential expression taking into account the initial contribution from the 450 nm intermediate. A time shift factor was used for the second rate of increase, associated explicitly with the isobestic conversion of the 340 nm intermediate to TPQ_{OX}. The absorbance changes from 0 to 2 ms were excluded from fits due to the very rapid increase or decrease in absorbance occurring at certain wavelengths during the dead time of the stopped-flow instrument.

RESULTS

Spectral Changes Associated with Single-Turnover Events at pH 7.2. The spectral changes accompanying reoxidation of fully reduced AGAO at pH 7.2 at 5 °C (Figure 1A), 10 °C (Figure 2A), and 20 °C (Figure S1A of the Supporting Information) establish that the reduced enzyme reacts rapidly with O_2 at 700 μM O_2. At 10 °C, the initial spectrum at 1.92 ms shows that the majority of the TPQ_{SQ} species has reacted by this time, based on the substantial decrease of the characteristic TPQ_{SQ} absorbance features at 436 and 466 nm. These features are no longer detectable after ~15 ms at 5 °C, whereas they disappear by ~3 ms at 20 °C. This is not surprising as reoxidation in general is significantly faster at 20 °C than at 5 and 10 °C (see below).

To more clearly differentiate reoxidation rates as a function of temperature, difference spectra were created by subtracting the final, fully oxidized TPQ_{OX} spectrum from each intermediate spectrum (see panels B and C of Figure 2 for examples). This allowed us to plot single-wavelength absorbance changes (Figure 1B,D and Figure S1B,D of the Supporting Information), enabling the determination of rate constants (Table S1 of the Supporting Information). At 700 μM O_2, the data reveal an extremely fast absorbance increase in the 325−375 nm region that occurs within the dead time of the stopped-flow instrument (Figure 2B). Despite the initial rapid increase in this region, the absorbance at 313.7 nm (Figure 1B,D and Figure S1B,D of the Supporting Information) decreases in single-exponential fashion over the course of the entire reaction under all experimental conditions tested.

On the basis of the difference spectra, the oxidative half-reaction appears to occur in two phases, as evidenced by the presence of two distinct isosbestic points. During the first ~20 ms of the reaction, spectral changes shift through an isosbestic point at ~385 nm (Figure 2B), whereas for the remainder of the half-reaction, spectral changes shift through an isosbestic point at ~392 nm (Figure 2C). These two isosbestic points are clearly resolved at both 5 and 10 °C, but only the second isosbestic point is apparent at 20 °C, because of the faster reoxidation kinetics at this temperature (Table S1). Notably, at all three temperatures, the rates of decay at 313 and 341 nm are essentially equivalent to the rate of increase at 499 nm (which reflects formation of TPQ_{OX}), and decay of the ~ 340 nm species is isosbestic with TPQ_{OX} formation (Figure 2C), which appears to be the rate-limiting step of the reaction.

The spectral changes accompanying reoxidation of fully reduced AGAO at pH 7.2 and 5 °C (Figure 1C), 10 °C (Figure 3A), or 20 °C (Figure S1C of the Supporting Information) at 150 μM O_2 closely resemble those described at 700 μM O_2. Indeed, the data conclusively show that the spectral changes are essentially identical between the two O_2 concentrations with one critical distinction. The characteristic TPQ_{SQ} absorbance bands at 436 and 466 nm in the first spectrum at 1.92 ms at 150 μM O_2 are significantly more intense than those observed at 700 μM O_2 (compare panels A and C of Figure 1 and Figure 2A to Figure 3A). Furthermore, over the course of the next ~25 ms, slight absorbance features at 436 and 466 nm are evident, indicating that the TPQ_{SQ} moiety is transiently present during reoxidation. These experiments also indicate that the observed rate constants at 313, 341, and 499 nm are essentially independent of oxygen concentration (Tables S1 and S2 of the Supporting Information). The one exception to this is the initial rate of increase at 450 nm (see Discussion), which is calculated to be roughly half of that observed at 700 μM O_2. Lastly, the spectral changes mimic the shift between the two isosbestic points as described for 700 μM O_2, with the first isosbestic point existing at ~380 nm during the first

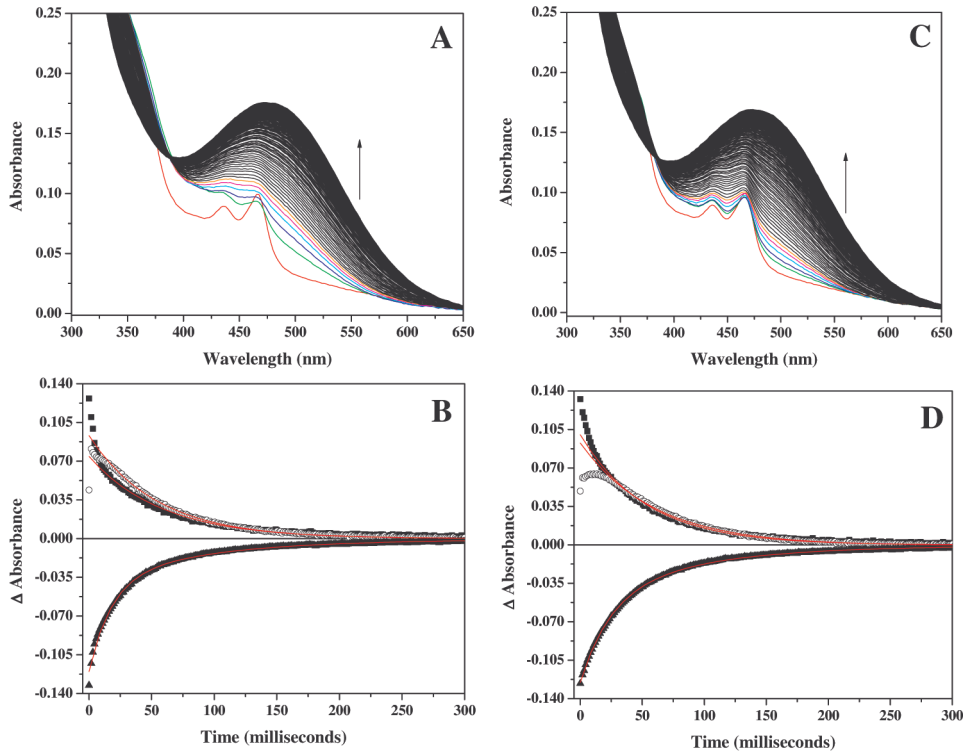

FIGURE 1: Stopped-flow spectral measurements of the reoxidation of reduced AGAO at 5 °C and pH 7.2. The protein concentration was 72 μM after mixing. (A) Observed spectral changes at 700 μM O_2. The following color scheme applies to panels A and C: red spectrum at 0 ms (see text), green spectrum at 1.92 ms, blue spectrum at 3.2 ms, cyan spectrum at 4.48 ms, magenta spectrum at 5.76 ms, and orange spectrum at 7.04 ms. Spectral changes from 8.32 to 500 ms are colored black. (B) Absorbance changes at fixed wavelengths from difference spectra at 700 μM O_2 with associated exponential fits (see Materials and Methods). The following single wavelengths are shown: 313.7 (■), 341.7 (○), and 499 nm (▲). (C) Observed spectral changes at 150 μM O_2. The protein concentration was 72 μM after mixing. (D) Absorbance changes at fixed wavelengths from difference spectra at 150 μM O_2 with associated exponential fits (see Materials and Methods). The following single wavelengths are shown: 313.7 (■), 341.7 (○), and 499 nm (▲).

~20 ms before shifting to the second isosbestic point at ~390 nm for the remainder of the oxidative half-reaction (data not shown).

Spectral Changes Associated with Single-Turnover Events at pH 8.2. Experiments conducted at 700 μM O_2 at pH 8.2 and 10 °C (Figure 2D) displayed spectral changes similar to those observed at pH 7.2, with three main exceptions. First, the 315 nm:340 nm absorbance ratio at 1.92 ms is ~1:1 at pH 8.2 (Figure 2E), whereas this ratio is ~1.25:1 at pH 7.2 (Figure 2B). Second, an initial, broader absorbance increase in the ~400 nm region is observed at pH 8.2 (Figure 2D). Finally, the presence of this new feature in the 400 nm region shifts the initial isosbestic point from ~385 nm at pH 7.2 to ~420 nm at pH 8.2 (compare panels B and E of Figure 2). The difference spectra are observed to shift through the 420 nm isosbestic point for ~8 ms before shifting to a second isosbestic point at ~390 nm for the remainder of the oxidative half-reaction (Figure 2F). Just as was the case at pH 7.2, slight absorbance features due to the TPQ_{SQ} are transiently present after the addition of O_2 and decay of the ~340 nm species is isosbestic with TPQ_{OX} formation and again appears to be the rate-limiting step of the reoxidation reaction. As shown in Table S1 of the Supporting Information, rates of decay at 313 and 341 nm are equal and are similar to the rate of increase at 488 nm (see below), the latter reflecting formation of TPQ_{OX}. The results indicate that the rate of TPQ_{OX} formation at pH 7.2 and 8.2 is virtually indistinguishable under our experimental conditions (Table S1).

The spectral changes accompanying reoxidation of fully reduced AGAO at pH 8.2 and 10 °C at 150 μM O_2 (Figure 3C) mimic those described at 150 μM O_2 at pH 7.2 and 10 °C but are distinct from the spectral changes described at 700 μM O_2 at pH 8.2. Note especially that the initial absorbance increase at 400 nm is less prevalent at lower O_2 levels; however, this absorbance is greater than that seen at pH 7.2 (Figure 3A,C). Additionally, whereas the 1.92 ms absorbance ratio of 315 nm to 340 nm is clearly ~1:1 at high O_2 levels at pH 8.2 (Figure 2E), this ratio becomes ~1.7:1 at 150 μM O_2 (Figure 3D), comparable to the ratio of ~1.4:1 observed at 150 μM O_2 and pH 7.2 (Figure 3B). Unlike the initial spectra at high O_2 levels, which cleanly shift through an isosbestic point at 420 nm, the difference spectra at 150 μM O_2 do not shift through any clear isosbestic point during the first few milliseconds of the reaction with O_2, but by ~10 ms, they are observed to shift through an isosbestic point at ~387 nm for the remainder of the oxidative half-reaction (data not shown).

The absorbance changes associated with the TPQ_{SQ} moiety during the initial phase of the reaction at pH 8.2 and 150 μM O_2 are similar to those observed for pH 7.2 at 150 μM O_2, again illustrating that the TPQ_{SQ} moiety is transiently present during reoxidation. Observed rate constants at 313, 341, and 488 nm for pH 8.2 are independent of oxygen concentration (Tables S1 and S2 of the Supporting Information). Once again, the one exception to this is the initial rate of increase at 450 nm which is observed to be roughly half of that calculated at 700 μM O_2.

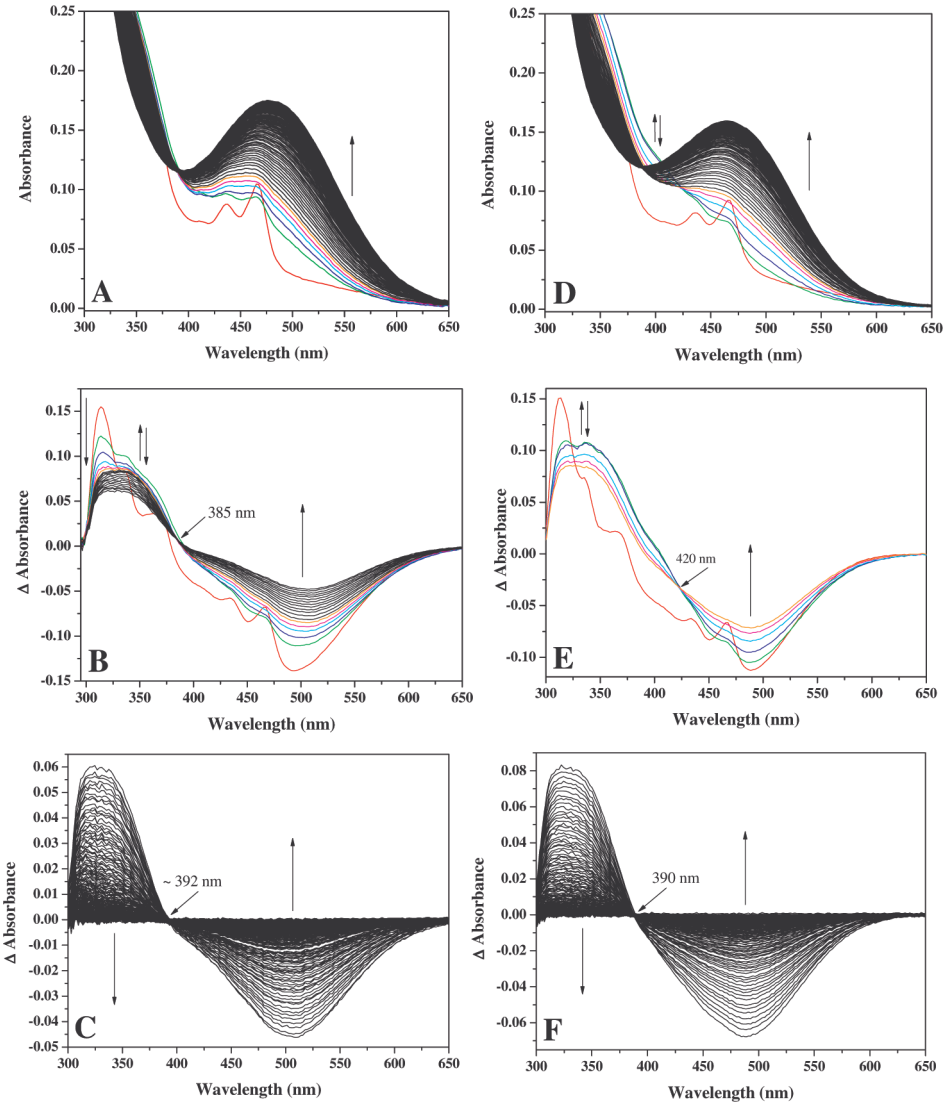

FIGURE 2: Stopped-flow spectral measurements of the reoxidation of reduced AGAO at 10 °C and 700 μM O_2. (A) Observed spectral changes at pH 7.2. The protein concentration was 71 μM after mixing. The following color scheme is identical for all spectra in this figure: red spectrum at 0 ms (see text), green spectrum at 1.92 ms, blue spectrum at 3.2 ms, cyan spectrum at 4.48 ms, magenta spectrum at 5.76 ms, and orange spectrum at 7.04 ms. Spectral changes from 8.32 to 500 ms are colored black. (B) pH 7.2 difference spectra created by subtracting the final oxidized TPQ spectrum at 500 ms from each intermediate spectrum. During the first ~20 ms of reoxidation, spectra shift through an isosbestic point at ~385 nm. (C) Difference spectra at pH 7.2 showing the spectral changes from 23 to 500 ms shifting through an isosbestic point at ~392 nm. (D) Observed spectral changes at pH 8.2. The protein concentration was 66 μM after mixing. (E) pH 8.2 difference spectra created by subtracting the final oxidized TPQ spectrum at 500 ms from each intermediate spectrum. During the first ~8 ms of reoxidation, spectra shift through an isosbestic point at 420 nm. (F) Difference spectra at pH 8.2 showing the spectral changes from 8.32 to 500 ms shifting through an isosbestic point at ~390 nm.

Spectral Changes Associated with Single-Turnover Events at pD 8.25. Reoxidation experiments at 700 μM O_2 at pD 8.25 and 10 °C (Figure S2A of the Supporting Information) yielded spectral changes similar to those observed at pH 8.2 with two main exceptions: (1) the initial 315 nm:340 nm absorbance ratio, which is ~1:1 at pH 8.2, becomes ~0.8:1 in D_2O (Figure S2C), and (2) an isotope effect is apparent. In agreement with previous findings (*41*), the absorbance at ~400 nm persists longer at pD 8.25 than at pH 8.2, due to the longer lifetime of a Cu−peroxy intermediate (see below), and results in the difference spectra shifting through an isosbestic point at ~424 nm for 16 ms (Figure S2C), at which point the spectra then shift through an isosbestic point at ~390 nm for the duration of the oxidative half-reaction (data not shown). As observed at pH 7.2 and 8.2, slight absorbance features due to the TPQ_{SQ} are transiently present following addition of O_2 and decay of the 340 nm species is isosbestic with TPQ_{OX} formation.

The second unique feature of the data collected in D_2O is the slower rate of increase at 488 nm (Table S1), corresponding to TPQ_{OX} formation, indicating a kinetic isotope effect is present. This observation concurs with that reported by Hirota et al. (*41*). The spectral changes accompanying reoxidation of reduced AGAO at pD 8.25 and 10 °C at 150 μM O_2 (Figure S2B) are similar to those described at pH 8.2 under the same experimental conditions.

Evidence of an O_2-Derived Intermediate. Hirota et al. observed the absorbance at 400 nm to be more prevalent in D_2O versus H_2O at basic pH at ~500 μM O_2, and this absorbance feature was assigned to a Cu−peroxy intermediate (*41*). The calculated rates of decay at 400 nm at pH 8.2

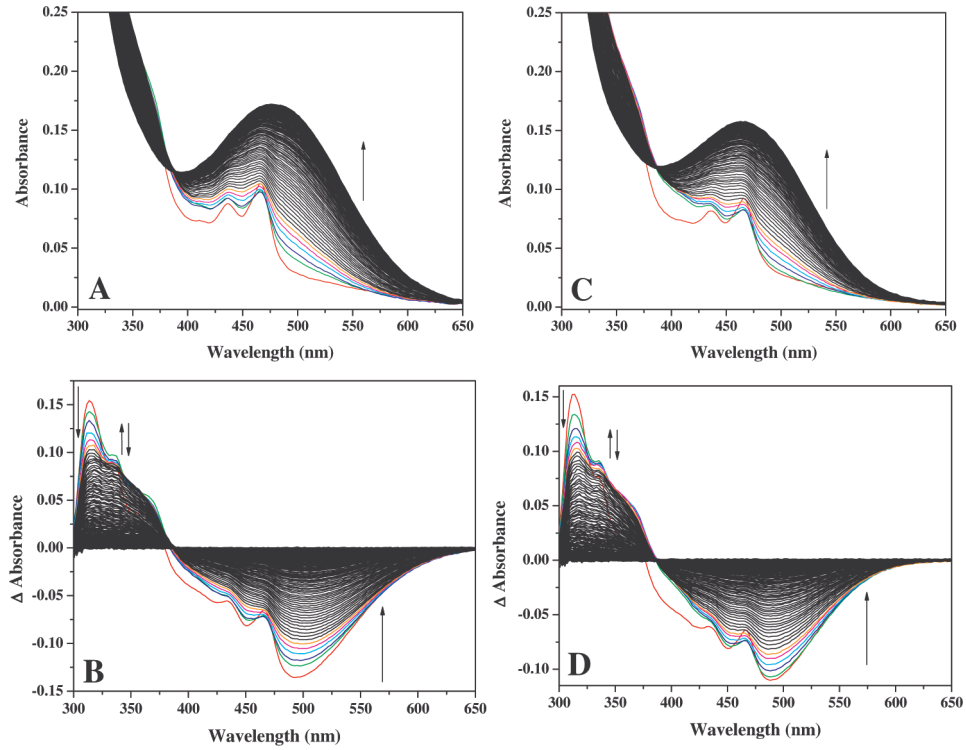

FIGURE 3: Stopped-flow spectral measurements of the reoxidation of reduced AGAO at 10 °C and 150 μM O_2. (A) Observed spectral changes at pH 7.2. The protein concentration was 71 μM after mixing. The following color scheme is identical for all spectra in this figure: red spectrum at 0 ms (see text), green spectrum at 1.92 ms, blue spectrum at 3.2 ms, cyan spectrum at 4.48 ms, magenta spectrum at 5.76 ms, and orange spectrum at 7.04 ms. Spectral changes from 8.32 to 500 ms are colored black. (B) pH 7.2 difference spectra created by subtracting the final oxidized TPQ spectrum at 500 ms from each intermediate spectrum. (C) Observed spectral changes at pH 8.2. The protein concentration was 66 μM after mixing. (D) pH 8.2 difference spectra created by subtracting the final oxidized TPQ spectrum at 500 ms from each intermediate spectrum.

and pD 8.25 reported in Table S1 are in excellent agreement with the rates of decay of this species reported in ref *41*.

The data presented in this report provide further evidence that this intermediate is indeed an O_2-derived species. A distinct feature at ~400 nm was observed only at saturating O_2 levels at pH 8.2 and pD 8.25 (Figure 2D and Figure S2A). This feature was much less prominent at 150 μM O_2, and absorbance changes at ~400 nm were simply too small to accurately determine k_{obs} for decay of this intermediate under these conditions. No absorbance increase was seen in this region for any of the experiments at pH 7.2, consistent with the hypothesis that the Cu−peroxy intermediate accumulates to a detectable level under basic conditions (*41*).

Global Data Analysis. Previous reports examining the oxidative half-reaction in AGAO provide an excellent framework for examining the current experimental results. For instance, it has been established that wild-type, copper-containing AGAO reacts extremely rapidly with O_2 in a non-rate-limiting fashion (apparent k_{obs} ~ 1000 s^{-1}) and that the rate-limiting step during reoxidation is formation of the charge-delocalized TPQ_{OX} cofactor via hydrolysis of the iminoquinone (*33, 41*). Furthermore, we have recently determined the intramolecular electron-transfer rate for the Cu(II)−TPQ_{AMQ} ⇆ Cu(I)−TPQ_{SQ} equilibrium in AGAO (*48*) (Table 1).

Along these lines, two mechanisms for reoxidation have been put forth and are summarized in Scheme 1. The key difference between these pathways is the identity of the species that reacts with O_2. In the top (inner-sphere) pathway (Scheme 1, **B** → **D**), Cu(I) is responsible for the first electron transfer to O_2, whereas in the bottom (outer-sphere) pathway (Scheme 1, **B2** → **D2**), the first electron-transfer event to O_2 occurs directly from TPQ_{AMQ}. To determine which mechanism is consistent with the data for AGAO, global analysis was utilized as a means of deconvoluting the rapid scan stopped-flow spectral changes.

Given this body of information, we tested the pathways outlined in Scheme 1. Inspection of the data provides some clear insights into the reaction of TPQ_{RED} with O_2. Most notably, the data collected at both O_2 concentrations under all experimental conditions show a very rapid disappearance (within the dead time of the stopped-flow instrument) in the majority of the absorbance features associated with TPQ_{SQ}. This permitted us to fix the pseudo-first-order rate constant for this kinetic step (TPQ_{RED} + O_2 → TPQ_{IMQ}) at ~1000 s^{-1} during global fitting analysis (note this would correspond to a second-order rate constant k_2 of 1.4 × 10^6 M^{-1} s^{-1}). Moreover, the spectral results clearly show the TPQ_{SQ} moiety to be transiently present following initial exposure to O_2, as evidenced by slight absorbance features at 436 and 466 nm. These absorbance features are present at both 700 and 150 μM O_2, although they are more pronounced and are apparent for a longer time period at lower oxygen levels, as expected for an intermediate that is reacting with O_2. Furthermore, under all experimental conditions, difference spectra clearly shift through an isosbestic point at ≈390 nm during the second, slower phase of the reoxidation reaction, showing the isosbestic conversion of an ~340 nm intermediate to TPQ_{OX} (Figure 2C,F).

Global modeling of the experimental data with two user-defined models (Scheme 1, **B** → **D** and **B2** → **D2**) establishes that the data are more consistent with the Cu(I)−TPQ_{SQ}

couple reacting with O_2, using a pseudo-first-order approximation for the reaction of Cu(I) with O_2 in eq 3. This difference is shown in Figure 4 which displays the calculated spectra from global modeling. It is important to note that, on the basis of the spectral changes associated with the TPQ_{SQ} moiety during the initial phase of reoxidation, Scheme 1 (**B** → **D**) is more consistent with the data because this pathway invokes a rapid reaction of Cu(I) with O_2 in a non-rate-limiting fashion.

The calculated spectra for the inner-sphere mechanism agree exceptionally well with the experimental data (compare Figure 2A to Figure 4A). In light of the rate constants in Table 1 and the experimental spectral changes, global modeling suggests that the majority of the Cu(I)−TPQ_{SQ} intermediate present in the fully reduced enzyme reacts upon exposure to O_2 within the dead time of the stopped-flow instrument. This result is consistent with the proposal that the interaction between Cu(I) and O_2 is not rate-limiting. It is very important to recognize that the rates of internal electron transfer between Cu(II)−TPQ_{AMQ} and Cu(I)−TPQ_{SQ} are slow relative to the rate of reaction with O_2. Hence, the reaction of these intermediates with O_2 can be distinguished. The transient presence of the TPQ_{SQ} absorbance features during the first few milliseconds of reoxidation is consistent with the formation of Cu(I)−TPQ_{SQ} from unreactive Cu(II)−TPQ_{AMQ} at a rate of 82 s^{-1} [eq 3; based on kinetic parameters for pH 7.2 and 10 °C (Table 1)], and its subsequent rapid reaction with O_2.

$$\underset{[TPQ_{AMQ}\text{- Cu(II)}]}{(\sim 72\ \mu M)} \underset{k_{-1} = 243\ s^{-1}}{\overset{k_{ET} = 82\ s^{-1}}{\rightleftharpoons}} \underset{[TPQ_{SQ}\text{- Cu(I)}]}{(\sim 26\ \mu M)} \xrightarrow[k_2 \sim 1000\ s^{-1}]{O_2} \underset{[TPQ_{IMQ}\text{ - Cu(II)-OOH}^-]}{} \quad (3)$$

$$\underset{[TPQ_{SQ}\text{- Cu(I)}]}{(\sim 26\ \mu M)} \underset{k_{ET} = 82\ s^{-1}}{\overset{k_1 = 243\ s^{-1}}{\rightleftharpoons}} \underset{[TPQ_{AMQ}\text{- Cu(II)}]}{(\sim 72\ \mu M)} \xrightarrow[k_2 \sim 22\ s^{-1}]{O_2,\ k_2 \sim 1000\ s^{-1}} \underset{[TPQ_{IMQ}\text{ - Cu(II)-OOH}^-]}{} \quad (4)$$

The high degree of similarity between the experimental and calculated spectra obtained when Cu(I)−TPQ_{SQ} is modeled as the reactive intermediate is in stark contrast to the calculated spectra obtained when Cu(II)−TPQ_{AMQ} is modeled as the reactive intermediate. As seen in Figure 4B, the calculated spectra show a substantially larger contribution from the TPQ_{SQ} absorbance features during the first 6 ms following O_2 exposure, which is unambiguously inconsistent with the experimental data. The experimentally measured k_{ET} of 243 s^{-1} between Cu(I) and TPQ_{SQ} to yield TPQ_{AMQ} (eq 4) is simply too low to account for the experimental spectral changes that occur within ~6 ms of O_2 introduction. Consequently, this model does not converge in the global analysis even if it is assumed that k_2 equals ~1000 s^{-1} (eq 4). However, the outer-sphere mechanism (Scheme 1, **B2** → **D2**) is predicated on the proposition that the reaction between TPQ_{AMQ} and O_2 is rate-limiting (*38*). When k_2 is modeled as the rate-limiting step (Table S1), the calculated spectra do not reproduce the observed spectra in any reasonable fashion (Figure 4C). Thus, the outer-sphere mechanism is simply inconsistent with the experimental data.

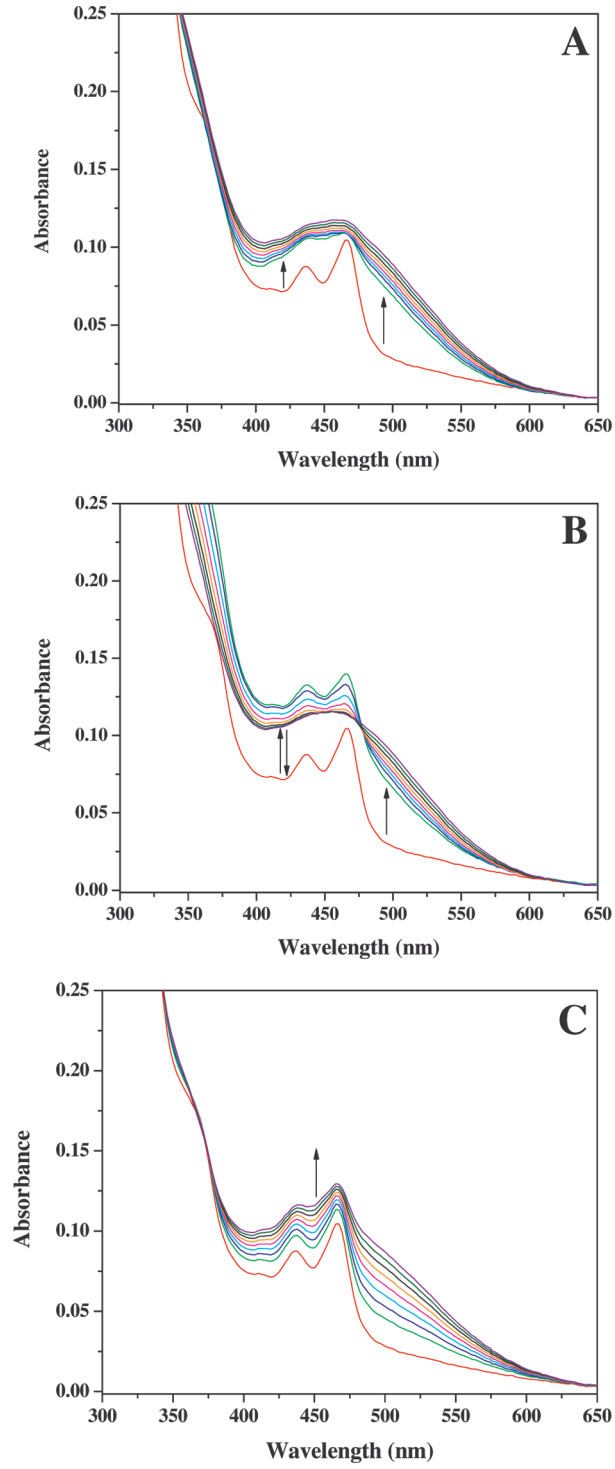

FIGURE 4: Select best fit modeled spectra calculated during global analysis for the 10 °C, pH 7.2, 700 μM O_2 experimental data set. (A) Calculated spectra from the user-defined model placing the TPQ_{SQ} moiety on-pathway, with the $k_{apparent}$ for the reaction of reduced enzyme with O_2 set to 1000 s^{-1} (eq 3). (B) Calculated spectra from the user-defined model placing the TPQ_{AMQ} moiety on-pathway, with the $k_{apparent}$ for the reaction of reduced enzyme with O_2 set to 1000 s^{-1} (eq 4). (C) Calculated spectra from the user-defined model placing the TPQ_{AMQ} moiety on-pathway, with the $k_{apparent}$ for the reaction of reduced enzyme with O_2 set to being equivalent with the rate-limiting step at 22 s^{-1} (eq 4, Table S1). The following color scheme is identical for all spectra in this figure. The red line represents the experimentally obtained spectrum of the reduced enzyme at 0 ms. All subsequent spectra are those generated during global analysis: green corresponding to 1.92 ms, blue to 3.2 ms, cyan to 4.48 ms, magenta to 5.76 ms, orange to 7.04 ms, black to 8.32 ms, olive to 9.6 ms, and violet to 10.88 ms.

Scheme 2: Revised CuAO Catalytic Mechanism for Cofactor Reoxidation in AGAO

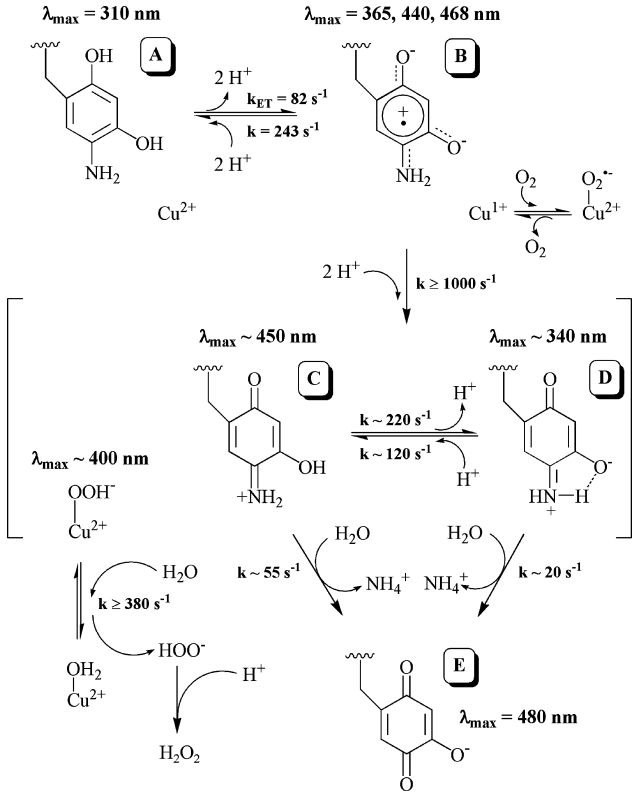

One of the major advantages of our approach compared to previous studies (*41*) is the ability to deconvolute the reduced enzyme spectrum (TPQ_{RED}) into component TPQ_{SQ} and TPQ_{AMQ} contributions. These individual components, along with their initial concentration values (prior to O_2 exposure), could then be fixed in global minimization routines. Rates for TPQ_{OX} formation were also entered for global analysis on the basis of double-exponential fits to absorbance changes (Tables S1 and S2) (see Materials and Methods). Rates of increase at 488 and 499 nm from these fits are less than rates of decrease at 341 nm, despite the isosbestic conversion of the 340 nm intermediate into TPQ_{OX} for all data sets. Given that three reactions contribute to the absorbance changes at 488 or 499 nm (formation of the 450 nm intermediate and its decay, formation of TPQ_{OX}), the error in the rates is larger than that estimated by the fitting routines. In fact, a single-exponential fit to the absorbance changes at 488 or 499 nm at longer times (when the 450 nm intermediate has largely been consumed) provides a good description of the data but larger rate constants, for example, 21.8 and 20.6 s^{-1} for the pH 7.2 and 10 °C data sets. For the global data analysis, we therefore approximated the rate associated with TPQ_{OX} formation by choosing intermediate values between calculated rates of decrease at 340 nm and rates of increase for TPQ_{OX} (pH 7.2, 5 °C, 15 s^{-1}; pH 7.2, 10 °C, 20 s^{-1}; pH 7.2, 20 °C, 50 s^{-1}; pH 8.2, 10 °C, 23 s^{-1}) (Tables S1 and S2).

As mentioned, all data sets show rate-limiting isosbestic conversion of an ~340 nm species to TPQ_{OX} (Figure 2C,F), providing strong evidence of the intramolecular hydrogen-bonded iminoquinone. Accordingly, a spectrum of this quinone intermediate (Scheme 2D, TPQ_{IMQ340}) as derived from model studies (*33*) was employed in the analysis. Fixing the spectra of TPQ_{SQ}, TPQ_{AMQ}, and TPQ_{IMQ340} resulted in the generation of the intermediate spectrum of a species with a broad absorption band with a λ_{max} of ~450 nm in all cases tested (see below). This result is consistent with an iminoquinone species lacking an intramolecular hydrogen bond, analogous to species **C** in Scheme 2 (TPQ_{IMQ450}) (see Discussion). Given this finding, several user-defined models involving the two forms of the iminoquinone were tested for their ability to fit the experimental data (Supporting Information). The model which best fit the experimental data suggested that oxidation of TPQ_{SQ} resulted in initial formation of TPQ_{IMQ450}, which is in equilibrium with TPQ_{IMQ340}, and both TPQ_{IMQ450} and TPQ_{IMQ340} hydrolyze to yield TPQ_{OX} (Scheme 2).

As discussed in the following section, ^{18}O kinetic isotope effects on the reoxidation reaction of PSAO (*51*) and AGAO (J. P. Roth and D. M. Dooley, unpublished results) are consistent with reversible binding of O_2 to Cu(I). Given these data, we tested a modification of our user-defined model allowing for the reversible binding of O_2 to Cu(I), with second-order rate constants of 1.4×10^6 M^{-1} s^{-1} at 700 μM O_2 and 6.6×10^6 M^{-1} s^{-1} at 150 μM O_2 (assumes $k_{obs} = 1000$ s^{-1}). The calculated spectra are in exceptional agreement with the 700 and 150 μM O_2 experimental data sets (compare Figure 5A to Figure 2A and Figure 5C to Figure 3A). Moreover, the absorption spectrum of the TPQ_{IMQ450} intermediate generated during global analysis is quite reasonable based on expectations from TPQ model chemistry (see Discussion) (Figure 5E). Convergence fails if the second-order rate is decreased to 2.8×10^4 M^{-1} s^{-1} (corresponding to a rate-limiting k_{obs} of 20 s^{-1}), lending further support to this model (Scheme 2).

Additionally, modeling the reversible binding of O_2 to Cu(I) offers an improvement in the spectra generated by global modeling, relative to the irreversible, first-order O_2 binding model (eq 3) (compare Figure 5A to Figure 4A). For the pH 7.2 and 700 μM O_2 experimental data set, residuals are ≈15% of the experimental spectral contribution at 1.92 ms (Figure S3A of the Supporting Information). The residuals decrease to ≤10% by 5.76 ms (Figure S3B), are ≤5% at 10.88 ms (Figure S3C), and are ≤2% at 16 ms (Figure S3D). Residuals for all subsequent spectra are ≤1% (data not shown). For the pH 7.2 and 150 μM O_2 experimental data set, the initial residuals at 1.92 ms are ≤10% of the experimental spectral contributions (Figure S4A of the Supporting Information). Residuals decrease to ≈7% by 5.76 ms (Figure S4B), are ≤5% at 10.88 ms (Figure S4C), and are ≤2% at 16 ms (Figure S4D). The residuals for all subsequent spectra are ≤1% (data not shown). In all cases, the calculated spectra quickly converge to the experimental data. The magnitudes of the residuals for the pH 7.2 and 5 °C data sets are nearly indistinguishable from those at 10 °C, while those obtained for the pH 7.2 and 20 °C data sets are ≤12% at 1.92 ms and quickly decrease to ≤1% (data not shown).

The only data sets which could not be modeled were those collected at pD 8.25 as the effect of D_2O on K_{eq} is unknown, as is the effect of D_2O on k_{ET} and k_{-1}. Regardless, the spectral changes are qualitatively very similar to those at pH 8.2. The pH 8.2 data at 700 μM O_2 were more difficult to analyze given the short-lived presence of the apparent Cu−OOH^- species absorbing at ~400 nm. The global model was

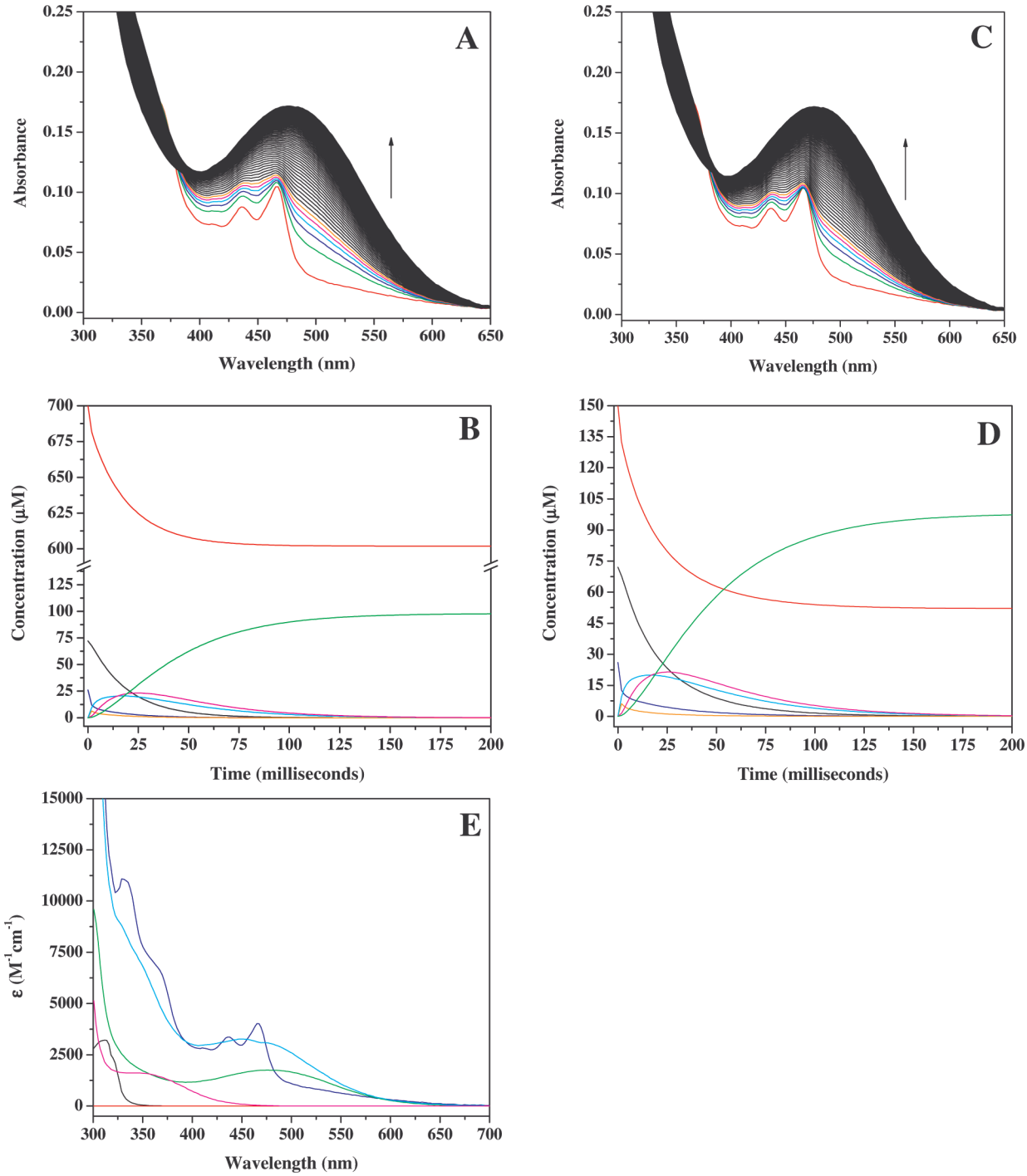

FIGURE 5: Best fit modeled spectra calculated during global analysis for the 10 °C and pH 7.2 experimental data sets. (A) Calculated spectra utilizing the model outlined in Scheme 2 with an initial O_2 concentration set at 700 μM. The following color scheme is identical for both panels A and C. The red line represents the experimentally obtained spectrum of the reduced enzyme at 0 ms. All subsequent spectra are those generated during global analysis: green corresponding to 1.92 ms, blue to 3.2 ms, cyan to 4.48 ms, magenta to 5.76 ms, and orange to 7.04 ms. All subsequent spectra in black represent the calculated, global analysis results for 8.32−500 ms. (B) Profiles ($[O_2]_{initial}$ = 700 μM) generated through global modeling detailing the concentration changes of each species over time. Species are as follows: Cu(II)−TPQ_{AMQ}, black; Cu(I)−TPQ_{SQ}, blue; O_2, red; Cu(II)−$O_2^{\bullet-}$−TPQ_{SQ}, orange; TPQ_{IMQ340}, magenta; TPQ_{IMQ450}, cyan; and TPQ_{OX}, green. (C) Calculated spectra utilizing the model outlined in Scheme 2 with the initial O_2 concentration set at 150 μM. (D) Profiles ($[O_2]_{initial}$ = 150 μM) generated through global modeling detailing the concentration changes of each species over time. Species are the same as in panel B. (E) Initial, intermediate, and product global analysis spectra. Species colors are the same as those in panel B except both the Cu(I)−TPQ_{SQ} and Cu(II)−$O_2^{\bullet-}$−TPQ_{SQ} moieties are colored blue as they have identical absorption properties.

modified to account for the rapid formation of this intermediate with a decay rate based on single-exponential fits (Table S1, 380 s^{-1}). Employing the kinetic rates in Table 1, global analysis showed that this model converged to the experimental data, although larger residuals were produced for initial spectra, relative to those observed for the pH 7.2 data.

At pH 8.2, the initial residuals are significantly larger, but the model satisfactorily reproduces the spectral contributions from ≥10 ms, yielding residuals at ~11 ms that are ≤10%, subsequently decreasing to ≤1% (data not shown). The large initial residuals in the 350−400 nm region can be attributed in part to the formation of the copper−peroxy species that

absorbs in the 400 nm region, as this intermediate does not accumulate at pH 7.2. Visual inspection of the experimental data at pH 8.2 does show that the initial absorbance in the 480 nm region is lower than that observed for the pH 7.2 data sets (compare panels A and D of Figure 2 and panels A and C of Figure 3), indicating that there is likely a pH sensitive step in the reaction that is not explicitly included in our model. Other models were evaluated but failed to improve the global fits (data not shown). Attempts to model the pH 8.2 and 700 μM O_2 data with a scheme that eliminated the 450 nm (protonated) quinone intermediate showed that the global model would not converge to the experimental data and the intermediate spectrum generated for the 350 nm quinone species had significant absorption in the 450 nm region, indicating that both the 350 and 450 nm intermediates form at pH 8.2. It should be noted that k_{ET} is pH sensitive and is decreased relative to that at pH 7.2 (*48*). As suggested in Scheme 2, there are multiple steps sensitive to pH and more work to sort out the mechanism in that level of detail remains.

DISCUSSION

Proposed Role of Copper in Reoxidation. Scheme 1 details the two pathways for the reoxidation of the substrate-reduced form of copper-containing amine oxidases. The essential distinction is whether the initial electron-transfer step occurs via an inner-sphere or outer-sphere pathway. The pathway outlined in the **B** → **D** step depicts the non-rate-limiting inner-sphere electron-transfer reaction between Cu(I) and O_2. Clearly, a critical step in this mechanism is the rate of electron transfer between TPQ_{AMQ} and Cu(II), which we have measured by temperature-jump relaxation in three amine oxidases, most recently in AGAO (*48*). These measurements establish that k_{ET} is greater than k_{cat} for the preferred substrate β-PEA at pH 6.2, 7.2, and 8.2, thereby permitting the Cu(I)−TPQ_{SQ} state to be a viable catalytic intermediate. Also, the magnitude of the forward and reverse electron-transfer rates permits the interconversion of the semiquinone and the aminoquinol to be observed on the stopped-flow time scale.

The outer-sphere mechanism outlined in Scheme 1 step **B2** → **D2** depicts the proposal for cofactor reoxidation when the copper center is not involved in the initial electron-transfer reaction. It has been suggested that O_2 binds in a hydrophobic pocket near the quinone cofactor, where it is subsequently reduced to $O_2^{\bullet-}$ by TPQ_{AMQ} in the rate-limiting step (**B2** → **C2**) (*38*). Despite these key mechanistic differences, both pathways converge at the copper-bound hydroperoxide, iminoquinone stage (species **E**).

Characterization of metal-substituted forms of CuAOs has proven to be a valuable approach to distinguishing the reoxidation mechanisms. Kinetics studies of Cu(II), Co(II), and Ni(II) forms of AGAO revealed that the $K_M(O_2)$ was virtually unchanged, whereas k_{cat} was drastically reduced when the native copper ion was substituted with either cobalt or nickel (*33*). This is in marked contrast to metal substitution studies with HPAO, where the significant reduction in activity observed for Co(II) was attributed to the 70-fold increase in $K_M(O_2)$, relative to that of the wild-type, copper-containing enzyme (*34, 35*). In the case of metal-substituted forms of AGAO, the reduction in k_{cat} was attributed to the initial reaction between TPQ_{AMQ} and O_2 being much slower in the metal-substituted enzymes (*33*), which implicates Cu(II) as playing an important role in the oxidative half-reaction. Kishishita et al. argued that the metal ion may bind superoxide and facilitate the second electron-transfer event (*33*). However, the significant rate enhancement observed for the native enzyme is also consistent with a rapid inner-sphere reaction between Cu(I) and O_2 that confers a kinetic advantage. We believed that a more careful analysis of the rapid spectral changes occurring following the introduction of O_2 would provide a more direct means of observing the potential reactivity of the Cu(I)−TPQ_{SQ} species, given the rates of the reversible, internal electron-transfer reaction and the distinctive absorbance spectrum of the semiquinone.

Mechanism of the Oxidative Half-Reaction in AGAO. Temperature jump kinetics studies allowed us to determine the rate of electron transfer between TPQ_{AMQ} and Cu(II) (*48*) and to resolve the kinetics parameters for the internal redox equilibrium presented in Table 1. Consequently, we could deconvolute the initial ($t = 0$ ms) TPQ_{RED} spectra into the component TPQ_{AMQ} and TPQ_{SQ} species and observe the reactivity of TPQ_{AMQ} versus TPQ_{SQ} through global data analysis, given the distinct spectral properties of these two quinone species. Global data analysis provides strong support for the inner-sphere mechanism, where Cu(I) in the Cu(I)−TPQ_{SQ} species reacts rapidly with O_2 (Figures 4 and 5). Accordingly, we present a mechanism for cofactor reoxidation in AGAO that invokes a redox role for the copper center (Scheme 2). This mechanism is fully consistent with all the experimental data presented herein as well as the metal substitution results in AGAO (*33*) but modifies the previous mechanism proposed in earlier stopped-flow work (*41*) (see the discussion below). Importantly, the inner-sphere mechanism is also fully consistent with the recent mechanistic studies and ^{18}O KIE measurements on the pea seedling amine oxidase (*51*), as well as the ^{18}O KIE measurements on AGAO, which indicate that O_2 binding is reversible (J. P. Roth and D. M. Dooley, unpublished results).

Inspection of the mechanism presented in Scheme 2 indicates that the rate of formation of TPQ_{IMQ450} (Scheme 2, **C**) should approximate k_{ET} following the rapid conversion of the "resting state" concentration of the Cu(I)−TPQ_{SQ} intermediate to the Cu(II)−OOH^-−TPQ_{IMQ450} moiety upon initial O_2 exposure, which predominately occurs in the dead time of the stopped-flow experiment. Following this "burst" phase with a k_{obs} of ~1000 s^{-1}, cofactor reoxidation proceeds through the conversion of unreactive Cu(II)−TPQ_{AMQ} into reactive Cu(I)−TPQ_{SQ} at a rate constant equivalent to k_{ET}, as the reaction of O_2 with the enzyme is not rate-limiting. Comparison of the rates of increase at 450 nm during the first 5−10 ms at 700 μM O_2 (Table S1) with the k_{ET} values in Table 1 shows reasonable agreement between these quantities. Moreover, inspection of experimental difference spectra clearly shows the disappearance of a feature with absorbance at ~310 nm during the initial phase of the oxidative half-reaction (Figures 2B,E and 3B,D). We believe this represents the conversion of the unreactive TPQ_{AMQ} moiety (absorbing at ~310 nm) into the reactive Cu(I)−TPQ_{SQ} species. The rate of decrease at 313 nm (Tables S1 and S2) likely does not equate to k_{ET} (Table 1) since three products of oxidation (TPQ_{IMQ450}, TPQ_{IMQ350}, and TPQ_{OX}) all have absorbance at ~310 nm (Figure 5E). Therefore, the rate of decrease at 313 nm obtained from

single-wavelength absorbance changes is probably an underestimation of the true decay rate of this feature. In contrast, the initial rate of change at 450 nm (Tables S1 and S2) can be analyzed more confidently because only TPQ_{IMQ450} and TPQ_{OX} absorb in this region and during the first ~10 ms of reoxidation the rate of change at 450 nm should be dominated by formation of TPQ_{IMQ450}.

Moreover, the data show that the TPQ_{SQ} absorbance features are more pronounced when O_2 levels approach the concentration of TPQ and copper (Figures 1C and 3A,C). The $K_M(O_2)$ in AGAO has been determined to be 33 ± 2 μM (*52*). When O_2 is not saturating (150 μM O_2 is ~4.5 × K_M), it is clear that a greater percentage of the available Cu(I)−TPQ_{SQ} in the resting enzyme does not completely react during the dead time of the stopped-flow instrument, compared to the reaction at 700 μM O_2 (~21 × K_M). Consequently, following initial exposure to O_2 the absorbance features due to the TPQ_{SQ} are more prevalent at 150 μM O_2 compared to that observed at 700 μM O_2 and persist for a longer period of time. At low O_2 concentrations, O_2-dependent steps may become partially rate-limiting such that the initial rate of increase at 450 nm (Table S2) no longer equates to k_{ET} (Table 1). These straightforward findings strongly support the inner-sphere mechanism for the reoxidation of substrate-reduced AGAO by O_2, as outlined in Scheme 2.

Subsequent Steps in Cofactor Reoxidation. Global analysis of experimental absorbance changes indicated that oxidation of TPQ_{SQ} results in formation of TPQ_{IMQ450}, which is in equilibrium with TPQ_{IMQ340}. Hydrolysis of this latter species corresponds to the rate-limiting formation of TPQ_{OX}. These assignments are consistent with several enzyme and model studies, particularly the demonstration that the neutral iminoquinone ($\lambda_{max} \approx 350$ nm) exists with the illustrated intramolecular hydrogen bond (*33, 53*) and that there is a substantial red shift in λ_{max} when this hydrogen bond is disrupted (*53*). Additionally, aeration of the aminophenol TPQ model compound resulted in formation of an iminoquinone species with a λ_{max} value of 448 nm, representing an iminoquinone lacking the intramolecular hydrogen bond (*47*). This result was substantiated by the observation of a similar λ_{max} when ammonia was added to resting BPAO (*47*). Furthermore, the existence of the TPQ_{IMQ340} moiety during single-turnover reoxidation conditions concurs with the flash-frozen structure of the steady-state species in ECAO (*39*). Single-crystal microspectrophotometry supported the iminoquinone assignment of TPQ in the crystals since the absorption spectrum was bleached ($\lambda_{max} \approx 350$ nm), consistent with a hydrogen-bonded iminoquinone (*33, 53*). Lastly, the observation that the difference spectra at pH 7.2 shift through the first isosbestic point for 20 ms whereas the pH 8.2 difference spectra shift through the first isosbestic point for only 8 ms may represent the fact that the 350 nm iminoquinone (proposed to be deprotonated) forms more regularly at basic pH (Figure 2). This spectroscopic evidence may independently substantiate the pH sensitive equilibrium in which the two iminoquinone species are proposed to exist (Scheme 2).

The kinetics of reoxidation at pD 8.25 suggest that the copper−hydroperoxide intermediate has a longer lifetime in D_2O, relative to that observed at pH 8.2 (Table S1). Additionally, the spectral changes associated with the rate of increase at 488 nm are significantly slower than those at pH 8.2. We suggest that the slowed rate of increase at 488 nm in deuterium, corresponding to a KIE, represents rate-limiting formation of the fully oxidized, charge-delocalized TPQ_{OX} moiety.

Comparison to Previous Stopped-Flow Studies of TPQ_{RED} Oxidation in AGAO. The previous stopped-flow study (*41*) of the reoxidation kinetics of reduced AGAO reported that the absorbance features of both the Cu(II)−TPQ_{AMQ} and Cu(I)−TPQ_{SQ} moieties disappeared within the dead time of the stopped-flow instrument. The products were suggested to be Cu−peroxy species absorbing at ~410 nm, and the protonated and deprotonated forms of the iminoquinone absorbing at 340 and 310 nm, respectively (*41*). However, the data were limited to a single temperature and one O_2 concentration. Moreover, complete TPQ reduction was typically not achieved as stoichiometric amounts of substrate were used to reduce TPQ_{OX}, and the spectra displayed a relatively low signal-to-noise ratio in the 300−320 nm region, which is a critical region for identifying intermediates in the reaction. Using the earlier studies as a solid foundation, we endeavored to extend and improve upon the results in several ways. First, cleaner single-turnover conditions were obtained by reducing the enzyme with excess substrate and separating the reduced enzyme from remaining substrate and aldehyde products immediately prior to experimentation. Second, our experimental design permitted us to acquire a true "time zero" spectrum of the reduced enzyme prior to addition of O_2. Third, we were able to deconvolute the reduced enzyme spectrum into TPQ_{AMQ} and TPQ_{SQ} component spectra and calculate the associated kinetics parameters for the various experimental conditions that were tested (Table 1; see Materials and Methods). Finally, and importantly, we obtained data at multiple temperatures, pH values, and O_2 concentrations.

Given the differences noted above, it is not surprising that in some instances our results do not completely concur with those reported previously (*41*). We believe this may be in part attributed to factors inherent to the rapid reaction of the Cu(I)−TPQ_{SQ} intermediate with O_2. Following the addition of O_2, the TPQ_{SQ} absorbance features make only a minor contribution to the observed spectra (Figures 1A and 2A,D). These features become readily observable at nonsaturating O_2 concentrations (Figures 1C and 3A,C). Because Hirota et al. examined reoxidation under only saturating O_2 conditions, it is quite reasonable that these slight absorbance features were simply missed, leading them to conclude that the absorbance features characteristic of both the TPQ_{AMQ} and TPQ_{SQ} moieties disappeared within the dead time of the stopped-flow instrument. Our results conclusively show this not to be the case.

Furthermore, Hirota et al. reported an absorbance increase at 310 nm over the first 20 ms of the oxidative half-reaction (*41*). Under all experimental conditions we tested, our data clearly show a clean, single-exponential decay at this wavelength (see Figure 1B,D and Figure S1B,D for examples). We were able to observe an absorbance increase at 310 nm during this time period only under multiple-turnover conditions, where product aldehydes were present (Figure S5A of the Supporting Information). In our attempts to identify the optimal conditions for achieving full TPQ_{OX} reduction and clean separation of excess β-PEA from AGAO,

stopped-flow data were collected from an enzyme sample which was reduced with 5 mM β-PEA. It was determined that at this relatively high concentration of β-PEA, complete separation from protein could not be achieved on the PD-10 column, resulting in trace amounts of amine and (probably) aldehydes present during reoxidation experiments (Figure S5A). None of the single-wavelength absorbance traces show single-exponential behavior during the first ~25 ms following O_2 introduction (Figure S5B). These results resemble those reported by Hirota et al., where "stoichoimetric" β-PEA was used to reduce TPQ_{OX}. The authors make note that incomplete TPQ reduction was sometimes observed. It is therefore possible that not all of the substrate reacted, such that trace amounts of β-PEA were present. Additionally, product aldehyde would have been present in these experiments. Either outcome, or both, could complicate the results. We also believe that the spectral assignments made by Hirota et al. for the two iminoquinone intermediates, which were based on spectral changes occurring during the first ~20 ms following addition of O_2 (*41*), are questionable. Conversely, the assignments in Scheme 2 are fully consistent with our results.

Conclusions. The stopped-flow kinetics, spectra, and global data analysis results provide strong evidence for an inner-sphere mechanism (Scheme 2) for the oxidative half-reaction in AGAO. While these data provide strong support for the catalytic viability of the Cu(I)−TPQ_{SQ} couple in AGAO, the kinetic competence of this moiety among CuAOs from other sources is not fully resolved. A substantial body of data establishes that the Cu(I)−TPQ_{SQ} intermediate reduces O_2 in the plant enzymes (*25, 31, 51, 52*). Furthermore, given the results and analysis in ref *51*, it is plausible that the Cu(I)−TPQ_{SQ} form is a catalytic intermediate more generally among CuAO enzymes, given the high degree of similarity in active site architecture. It might be possible that CuAOs from different sources utilize distinct mechanisms of TPQ_{RED} oxidation, and this possibility may need to be evaluated on a case-by-case basis. Indeed, it appears possible that an outer-sphere mechanism operates in the Co(II)- and Ni(II)-substituted forms of AGAO, although with rate constants that are ~1% of that of the native, Cu(II)-containing enzyme (*33*). In any event, the data presented herein demonstrate that the active site environment in native AGAO has been tuned to exploit the reactivity of Cu(I)−TPQ_{SQ}.

ACKNOWLEDGMENT

We are grateful to Kimberly M. Hilmer for purifying the AGAO used in the pH 7.2 and 5 °C stopped-flow experiments and to Jonathan K. Hilmer for helpful discussions about global data analysis. We thank Doreen E. Brown for titrating substrate-reduced AGAO with cyanide for the determination of the TPQ_{SQ} ε_{468} value. We thank Professor Minae Mure (Kansas State University, Manhattan, KS) for helpful discussions concerning the proposed reoxidation mechanism.

SUPPORTING INFORMATION AVAILABLE

Rate constants during single-turnover reoxidation of reduced AGAO at 700 μM O_2 (Table S1) and 150 μM O_2 (Table S2), stopped-flow spectral measurements of reoxidation at 20 °C, pH 7.2, and 700 μM O_2 (Figure S1A) and 150 μM O_2 (Figure S1C) along with respective absorbance changes at fixed wavelengths (Figure S5B,D), stopped-flow spectral measurements of reoxidation at 10 °C, pD 8.25, and 700 μM O_2 (Figure S2A) and 150 μM O_2 (Figure S2B) and associated difference spectra for 700 μM O_2 data (Figure S2C), description of the user-defined models involving the two forms of the iminoquinone which were used to fit experimental data (Supplementary Results), overlay of experimental pH 7.2 and 10 °C data with associated best fit model spectra generated through global analysis and associated residuals for 700 μM O_2 at four time points (Figure S3A−D) and 150 μM O_2 at four time points (Figure S4A−D), and stopped-flow spectral measurements of reoxidation at 10 °C, pH 7.2, and 700 μM O_2 under multiple-turnover conditions (Figure S5A) with associated absorbance changes at fixed wavelengths (Figure S5B). This material is available free of charge via the Internet at http://pubs.acs.org.

NOTE ADDED IN PROOF

Additional best fit modeled spectra generated through global analysis using different second-order rate constants have been added to Supporting Information (Figures S6A and S6B). These calculated spectra further establish that the global model outlined in Scheme 2 converges to the experimental data under a range of rate constants for the rapid reaction of the [Cu(I)–TPQ_{SQ}] moiety with O_2 under saturating and non-saturating conditions.

REFERENCES

1. Ruggiero, C. E., and Dooley, D. M. (1999) Stoichiometry of the topa quinone biogenesis reaction in copper amine oxidases. *Biochemistry 38*, 2892–2898.
2. Ruggiero, C. E., Smith, J. A., Tanizawa, K., and Dooley, D. M. (1997) Mechanistic studies of topa quinone biogenesis in phenylethylamine oxidase. *Biochemistry 36*, 1953–1959.
3. Bollinger, J. A., Brown, D. E., and Dooley, D. M. (2005) The formation of lysyltyrosine quinone (LTQ) is a self-processing reaction. Expression and characterization of a *Drosophila* lysyl oxidase. *Biochemistry 44*, 11708–11714.
4. DuBois, J. L., and Klinman, J. P. (2005) Mechanism of post-translational quinone formation in copper amine oxidases and its relationship to the catalytic turnover. *Arch. Biochem. Biophys. 433*, 255–265.
5. Elmore, B., Bollinger, J. A., and Dooley, D. M. (2002) Human kidney diamine oxidase: Heterologous expression, purification, and characterization. *J. Biol. Inorg. Chem. 7*, 565–579.
6. Carter, S. R., McGuirl, M. A., Brown, D. E., and Dooley, D. M. (1994) Purification and active-site characterization of equine plasma amine oxidase. *J. Inorg. Biochem. 56*, 127–141.
7. McIntire, W. S., and Hartmann, C. (1993) Copper-Containing Amine Oxidases. In *Principles and Applications of Quinoproteins* (Davidson, V. L., Ed.) pp 97−171, Marcel Dekker Inc., New York.
8. Mercier, N., Moldes, M., El Hadri, K., and Fève, B. (2003) Regulation of semicarbazide-sensitive amine oxidase expression by tumor necrosis factor-α in adipocytes: Functional consequences on glucose transport. *J. Pharmacol. Exp. Ther. 304*, 1197–1208.
9. Yu, P. H., Wright, S., Fan, E. H., Lun, Z. R., and Gubisne-Harberle, D. (2003) Physiological and pathological implications of semicarbazide-sensitive amine oxidase. *Biochim. Biophys. Acta 1647*, 193–199.
10. Boomsma, F., Bhaggoe, U. M., Van der Houwen, A. M. B., and Van den Meiracker, A. H. (2003) Plasma semicarbazide-sensitive amine oxidase in human (patho)physiology. *Biochim. Biophys. Acta 1647*, 48–54.
11. O'Sullivan, J., Unzeta, M., Healy, J., O'Sullivan, M. I., Davey, G., and Tipton, K. F. (2004) Semicarbazide-sensitive amine oxidases: Enzymes with quite a lot to do. *Neurotoxicology 25*, 303–315.
12. Matyus, P., Dajka-Halasz, B., Foldi, A., Haider, N., Barlocco, D., and Magyar, K. (2004) Semicarbazide-sensitive amine oxidase: Current status and perspectives. *Curr. Med. Chem. 11*, 1285–1298.

13. Parsons, M. R., Convery, M. A., Wilmot, C. M., Yadav, K. D. S., Blakeley, V., Corner, A. S., Phillips, S. E. V., McPherson, M. J., and Knowles, P. F. (1995) Crystal structure of a quinoenzyme: Copper amine oxidase of *Escherichia coli* at 2 Å resolution. *Structure 3*, 1171–1184.
14. Kumar, V., Dooley, D. M., Freeman, H. C., Guss, J. M., Harvey, I., McGuirl, M. A., Wilce, M. C. J., and Zubak, V. M. (1996) Crystal structure of a eukaryotic (pea seedling) copper-containing amine oxidase at 2.2 Å resolution. *Structure 4*, 943–955.
15. Wilce, M. C. J., Dooley, D. M., Freeman, H. C., Guss, J. M., Matsunami, H., McIntire, W. S., Ruggiero, C. E., Tanizawa, K., and Yamaguchi, H. (1997) Crystal structures of the copper-containing amine oxidase from *Arthrobacter globiformis* in the holo and apo forms: Implications for the biogenesis of topaquinone. *Biochemistry 36*, 16116–16133.
16. Li, R. B., Klinman, J. P., and Mathews, F. S. (1998) Copper amine oxidase from *Hansenula polymorpha*: The crystal structure determined at 2.4 Å resolution reveals the active conformation. *Structure 6*, 293–307.
17. Duff, A. P., Cohen, A. E., Ellis, P. J., Kuchar, J. A., Langley, D. B., Shepard, E. M., Dooley, D. M., Freeman, H. C., and Guss, J. M. (2003) The crystal structure of *Pichia pastoris* lysyl oxidase. *Biochemistry 42*, 15148–15157.
18. Lunelli, M., Di Paolo, M. L., Biadene, M., Calderone, V., Battistutta, R., Scarpa, M., Rigo, A., and Zanotti, G. (2005) Crystal structure of amine oxidase from bovine serum. *J. Mol. Biol. 346*, 991–1004.
19. Chen, Z. W., Schwartz, B., Williams, N. K., Li, R. B., Klinman, J. P., and Mathews, F. S. (2000) Crystal structure at 2.5 Å resolution of zinc-substituted copper amine oxidase of *Hansenula polymorpha* expressed in *Escherichia coli*. *Biochemistry 39*, 9709–9717.
20. O'Connell, K. M., Langley, D. B., Shepard, E. M., Duff, A. P., Jeon, H. B., Sun, G., Freeman, H. C., Guss, J. M., Sayre, L. M., and Dooley, D. M. (2004) Differential inhibition of six copper amine oxidases by a family of 4-(aryloxy)-2-butynamines: Evidence for a new mode of inactivation. *Biochemistry 43*, 10965–10978.
21. Dove, J. E., and Klinman, J. P. (2001) Trihydroxyphenylalanine quinone (TPQ) from copper amine oxidases and lysyl tyrosylquinone (LTQ) from lysyl oxidase. *Adv. Protein Chem. 58*, 141–174.
22. Dawkes, H. C., and Phillips, S. E. V. (2001) Copper amine oxidase: Cunning cofactor and controversial copper. *Curr. Opin. Struct. Biol. 11*, 666–673.
23. Halcrow, M., Phillips, S., and Knowles, P. (2000) Amine Oxidases and Galactose Oxidase. In *Subcellular Biochemistry* (Holzenburg, A., and Scrutton, N., Eds.) pp 183−231, Kluwer Academic/Plenum Publishers, New York.
24. Dooley, D. M., McGuirl, M. A., Brown, D. E., Turowski, P. N., McIntire, W. S., and Knowles, P. F. (1991) A Cu(I)-semiquinone state in substrate-reduced amine oxidases. *Nature 349*, 262–264.
25. Turowski, P. N., McGuirl, M. A., and Dooley, D. M. (1993) Intramolecular electron transfer rate between active-site copper and topa quinone in pea seedling amine oxidase. *J. Biol. Chem. 268*, 17680–17682.
26. Dooley, D. M., and Brown, D. E. (1996) Intramolecular electron transfer in the oxidation of amines by methylamine oxidase from *Arthrobacter P1*. *J. Biol. Inorg. Chem. 1*, 205–209.
27. Ho, R. Y. N., Liebman, J. F., and Valentine, J. S. (1995) Overview of the Energetics and Reactivity of Oxygen. In *Active Oxygen in Chemistry* (Foote, C. S., Valentine, J. S., Greenberg, A., and Liebman, J. F., Eds.) pp 1−23, Blackie Academic and Professional, New York.
28. Murthy, N. N., and Karlin, K. D. (1995) in *Mechanistic Bioinorganic Chemistry* (Thorp, H. H., and Pecoraro, V. L., Eds.) pp 165−193, American Chemical Society, Washington, DC.
29. Karlin, K. D., and Tyekl'ar, Z. (1993) *Bioinorganic Chemistry of Copper*, Chapman and Hall, New York.
30. Whittaker, J. W. (1999) Oxygen reactions of the copper oxidases. *Essays Biochem. 34*, 155–172.
31. Medda, R., Padiglia, A., Bellelli, A., Sarti, P., Santanche, S., Agro, A. F., and Floris, G. (1998) Intermediates in the catalytic cycle of lentil (*Lens esculenta*) seedling copper-containing amine oxidase. *Biochem. J. 332*, 431–437.
32. Padiglia, A., Medda, R., Bellelli, A., Agostinelli, E., Morpurgo, L., Mondovi, B., Finazzi-Agrò, A., and Floris, G. (2001) The reductive and oxidative half-reaction and the role of copper ions in plant and mammalian copper-amine oxidases. *Eur. J. Inorg. Chem. 1*, 35–42.
33. Kishishita, S., Okajima, T., Kim, M., Yamaguchi, H., Hirota, S., Suzuki, S., Kuroda, S., Tanizawa, K., and Mure, M. (2003) Role of copper ion in bacterial copper amine oxidase: Spectroscopic and crystallographic studies of metal-substituted enzymes. *J. Am. Chem. Soc. 125*, 1041–1055.
34. Mills, S. A., and Klinman, J. P. (2000) Evidence against reduction of Cu^{2+} to Cu^{+} during dioxygen activation in a copper amine oxidase from yeast. *J. Am. Chem. Soc. 122*, 9897–9904.
35. Mills, S. A., Goto, Y., Su, Q. J., Plastino, J., and Klinman, J. P. (2002) Mechanistic comparison of the cobalt-substituted and wild-type copper amine oxidase from *Hansenula polymorpha*. *Biochemistry 41*, 10577–10584.
36. Schwartz, B., Olgin, A. K., and Klinman, J. P. (2001) The role of copper in topa quinone biogenesis and catalysis, as probed by azide inhibition of a copper amine oxidase from yeast. *Biochemistry 40*, 2954–2963.
37. Su, Q. J., and Klinman, J. P. (1998) Probing the mechanism of proton coupled electron transfer to dioxygen: The oxidative half-reaction of bovine serum amine oxidase. *Biochemistry 37*, 12513–12525.
38. Mure, M., Mills, S. A., and Klinman, J. P. (2002) Catalytic mechanism of the topa quinone containing copper amine oxidases. *Biochemistry 41*, 9269–9278.
39. Wilmot, C. M., Hajdu, J., McPherson, M. J., Knowles, P. F., and Phillips, S. E. V. (1999) Visualization of dioxygen bound to copper during enzyme catalysis. *Science 286*, 1724–1728.
40. Brazeau, B. J., Johnson, B. J., and Wilmot, C. M. (2004) Copper-containing amine oxidases. Biogenesis and catalysis; a structural perspective. *Arch. Biochem. Biophys. 428*, 22–31.
41. Hirota, S., Iwamoto, T., Kishishita, S., Okajima, T., Yamauchi, O., and Tanizawa, K. (2001) Spectroscopic observation of intermediates formed during the oxidative half-reaction of copper/topa quinone-containing phenylethylamine oxidase. *Biochemistry 40*, 15789–15796.
42. Juda, G. A., Bollinger, J. A., and Dooley, D. M. (2001) Construction, overexpression, and purification of *Arthrobacter globiformis* amine oxidase: Strep-Tag II fusion protein. *Protein Expression Purif. 22*, 455–461.
43. Janes, S. M., and Klinman, J. P. (1991) An investigation of bovine serum amine oxidase active site stoichiometry: Evidence for an aminotransferase mechanism involving two carbonyl cofactors per enzyme dimer. *Biochemistry 30*, 4599–4605.
44. Meites, L., and Meites, T. (1948) Removal of oxygen from gas streams. *Anal. Chem. 20*, 984–985.
45. Weiss, R. (1970) The solubility of nitrogen, oxygen, and argon in water and seawater. *Deep Sea Res. 17*, 721–735.
46. Medda, R., Padiglia, A., Bellelli, A., Pedersen, J. Z., Agro, A. F., and Floris, G. (1999) Cu(I)-semiquinone radical species in plant copper-amine oxidases. *FEBS Lett. 453*, 1–5.
47. Mure, M., and Klinman, J. P. (1993) Synthesis and spectroscopic characterization of model compounds for the active site cofactor in copper amine oxidases. *J. Am. Chem. Soc. 115*, 7117–7127.
48. Shepard, E. M., and Dooley, D. M. (2006) Intramolecular electron transfer rate between active-site copper and TPQ in *Arthrobacter globiformis* amine oxidase. *J. Biol. Inorg. Chem. 11*, 1039–1048.
49. Shepard, E. M., Juda, G. A., Ling, K. Q., Sayre, L. M., and Dooley, D. M. (2004) Cyanide as a copper and quinone-directed inhibitor of amine oxidases from pea seedlings (*Pisum sativum*) and *Arthrobacter globiformis*: Evidence for both copper coordination and cyanohydrin derivatization of the quinone cofactor. *J. Biol. Inorg. Chem. 9*, 256–268.
50. Chiu, Y. C., Okajima, T., Murakawa, T., Uchida, M., Taki, M., Hirota, S., Kim, M., Yamaguchi, H., Kawano, Y., Kamiya, N., Kuroda, S., Hayashi, H., Yamamoto, Y., and Tanizawa, K. (2006) Kinetic and structural studies on the catalytic role of the aspartic acid residue conserved in copper amine oxidase. *Biochemistry 45*, 4105–4120.
51. Mukherjee, A., Smirnov, V. V., Lanci, M. P., Brown, D. E., Shepard, E. M., Dooley, D. M., and Roth, J. P. (2008) Inner-sphere mechanism for molecular oxygen reduction catalyzed by copper amine oxidases. *J. Am. Chem. Soc. 130*, 9459–9473.
52. Juda, G. A., Shepard, E. M., Elmore, B. O., and Dooley, D. M. (2006) A comparative study of the binding and inhibition of four copper containing amine oxidases by azide: Implications for the role of copper during the oxidative half-reaction. *Biochemistry 45*, 8788–8800.
53. Mure, M., and Klinman, J. P. (1995) Model studies of topaquinone-dependent amine oxidases. Characterization of reaction intermediates and mechanism. *J. Am. Chem. Soc. 117*, 8707–8718.

BI8011516